HiSST: International Conference on High-Speed Vehicle Science Technology
26–29 November 2018, Moscow, Russia

Preliminary Design of a Hooded Fairing Accommodating Winged Payloads

Jeroen Van den Eynde[1], Attila Jasko[2], João F. A. Martos[1,3], Matteo Appolloni[2], Johan Steelant[1], Alexander Kallenbach[4], Anton Shardin[5], Anton Gorskiy[5]

Abstract

To accommodate the protruding wing tips and control surfaces under the fairing of a sounding rocket, a hooded fairing is proposed by DLR avoiding as such the use of an oversized hammerhead fairing. The latter would induce a larger aerodynamic drag and lower the static margin significantly. To assure a symmetric configuration, a third hood is added such that the hoods are azimuthally 120° separated. This particular fairing configuration opens up the possibility to accommodate larger dimensions of flight test vehicles otherwise limited by the finite wing span.

Due to the cut-outs in the monocoque fairing allowing the passage of the wing tips and control surfaces, one reduces locally the stiffness and introduces local stresses. Furthermore, during the fairing release by forward translation, a guidance reduces uncontrolled attitude changes of the cone and prevents unwanted impact of the hoods and cone with the wingtips and payload.

The preliminary design will further consider the various loads to which the fairing is exposed to from lift-off up to fairing release at 75km altitude 121 seconds later. As the flight follows a suppressed trajectory, the longer passage in the atmosphere results in an extended exposure to thermo-mechanical loads. This entails mechanical vibration, acceleration, aerodynamic and thermal loads. Based upon the thermo-mechanical analyses, the shell thickness and the material choice will be optimized. Glass fibre composite is the basic material of choice as it is transparent for Radio Frequency.

Keywords: *Fairing, Winged payload, CFD, Hypersonic, FEA*

Nomenclature

AoA – Angle of Attack
h – Heat transfer coefficient
C_l – Lift force coefficient
C_d – Drag force coefficient
C_m – Moment coefficient
C_p – Coefficient of pressure
CFD – Computational Fluid Dynamics
DLR – Deutsches Zentrum für Luft- und Raumfahrt (German Aerospace Center)
DoF – Degrees of freedom
EFTV – Experimental Flight Test Vehicle
FEA – Finite-element Analysis
FEM – Finite-element Model
h – Heat transfer coefficient
HXI – High Speed Experimental Fly Vehicles - International
LVSM – Launch Vehicle Service Module
M – Mach Number
MPC – Multi-Point Constraints
PEEK - PolyEtherEtherKetone
Q_{max} – Maximum dynamic pressure
Re – Reynolds Number
ST – Shock tunnel
St – Stanton Number

[1] *ESA/ESTEC, Flight Vehicles and Aerothermodynamics Engineering Section, 2200AG Noordwijk, The Netherlands (Jeroen.Van.den.Eynde@esa.int; Johan.Steelant@esa.int)*
[2] *ESA/ESTEC, Engineering Services Section, 2200AG Noordwijk, The Netherlands (Attila.Jasko@esa.int; Matteo.Appolloni@esa.int)*
[3] *Institute for Advanced Studies, Division of Aerothermodynamics and Hypersonics, São José dos Campos, SP, Brazil (joaomartos@gmail.com)*
[4] *German Aerospace Center, Mobile Rocket Base, Oberpfaffenhofen, 82234 Wessling, Germany, DLR-Moraba (Alexander.Kallenbach@dlr.de)*
[5] *Central Aerohydrodynamic Institute (TsAGI), Research and Production Complex, Zhukovsky, Moscow region, 140180 Russia (ao_shardin@tsagi.ru; anton.gorskiy@tsagi.ru)*

1. Introduction

Testing of high-speed vehicles or its components by means of sounding rockets have become common practice [2,3,4,5,6]. If required, the payloads are mounted underneath a nose cone or fairing to protect the payload during the ascent phase within the atmosphere or to enable the flight of axially asymmetric payload shapes on unguided sounding rockets. Simple geometries such as cones or wedges can be exposed to the atmosphere during ascent allowing the collection of data during both ascent and descent. In case of a complex geometry, e.g. a winged vehicle, this option is not viable as it endangers the longitudinal stability of the sounding rocket. The fairing has then also the function to eliminate any lateral and asymmetric aerodynamics forces induced by the payload.

Sounding rockets usually pass through the dense atmosphere quickly. The related aerodynamic and thermal loads play a very important role in its preliminary design along with those generated by vibrational and acoustic loads induced by the motor. Since the flow properties along the trajectory changes quickly, the aerothermal analysis should be transient according to the vehicle trajectory, whereas the vibrations can be assessed by quasi-static load analysis.

An additional complexity arises when dealing with oversized payloads. The mass and dimensions of the flight test vehicle are limited by the launcher capability, specifically the available volume under the fairing. Already for small span vehicles, the fairing diameter limits the overall size of the vehicle. To circumvent this restriction, an alternative solution is to let the wing span cross the fairing's periphery and having hoods mounted onto the outside of the fairing to protect the wings during ascent and to avoid aerodynamic lift generation at the forward side rocket. Consequently, the fairing diameter accommodates the vehicle main body and the hoods cover the outer parts of the wing span depassing the fairing diameter (Fig 1). The hoods are dimensioned such that they avoid aerodynamic lift generation in nominal conditions, i.e. AoA=0°.

An extensive numerical aerothermodynamics analysis based on the VBS-43 trajectory has been performed for the proposed hooded fairing and is presented in [1]. These aero-thermal database provides the necessary pressure and thermal loads for a preliminary design of this hooded fairing.

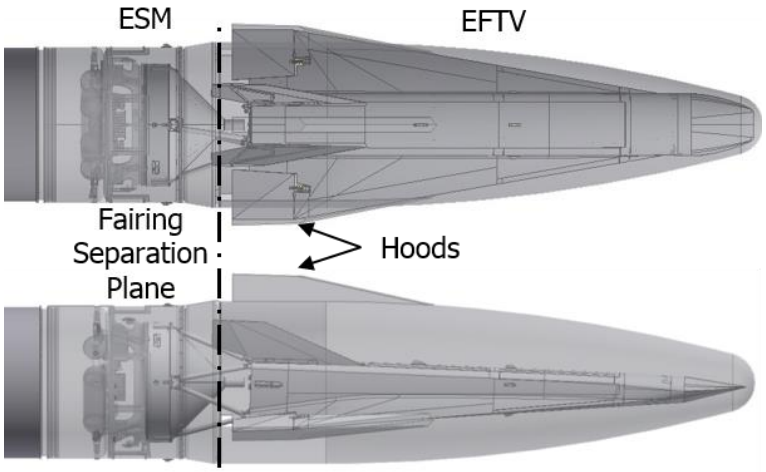

Fig 1. Fairing flight model sketch.

The overall shape of the hooded fairing is defined by the HEXAFLY-INT mission which is a free flight glider testing an innovative high-speed waverider with several breakthrough technologies on board. This approach will create the basis to gradually increase the TRL level relevant to the design of hypersonic vehicles. The Experimental Flight Test Vehicle (EFTV) was conceived to achieve a level flight at an altitude of about 32 km, after a pull-out manoeuvre during the downleg of a suppressed trajectory [6]. However, for the preliminary design of the fairing, only the ascending part of the ballistic flight is of interest until fairing release. The VBS-43 single-stage launch vehicle lifts off in vertical position from a launch stool in CLA (Alcântara). A pitch over manoeuvre induces a suppressed trajectory. The VBS-43 burns out at 65s which is below 40km altitude, fins passively stabilize the vehicle and an active cold

gas system provides rate and attitude control at high altitude in the jet-off flight phase. Fairing release shall be above 75km altitude by inducing a delta velocity forward.

The detailed design, structural analysis and manufacturing of the fairing requires a complete aero-thermal load analysis considering the maximum loads during flight (transonic flight and highest dynamic pressure) and transient conjugated heat transfer analysis through the trajectory. The shock waves generated in the vicinity of the hoods' surface increase significantly the thermal loads in this area and should be also considered. In addition, it is necessary to prevent that the surface heat loads affects the payload. The aerothermodynamics data-base will be generated by numerically simulations for critical points in the flight trajectory.

The results of the aerothermodynamic simulations serve as an input for the finite-element analysis of the fairing. Deformations and stresses have been calculated by static analyses. The eigenmodes of the fairing and the EFTV-ESM-LVSM-Fairing stack have been calculated using normal modes analyses. The results of these analyses are used for the final design of the fairing.

2. Aerodynamic Loads and Heat Flux along Trajectory

Based on the VBS-43 trajectory, it is possible to extract the critical points for the aerothermal analysis involving transonic flight, highest dynamic pressure and dense atmosphere (Fig 2). Aerothermodynamics data-base were based on the critical points described in Table 1. The CFD simulations were performed for Mach number around 0.29 to 8.02 and altitude around 0 to 45 km considering isothermal cold wall (300 K). The aerothermodynamic data-base provides the fairing thermal loading by means of surface heat flux distributions and pressure loads. This provides the necessary information to provide the expected heat and pressure loads essential for the fairing's structural and thermal design.

A detailed description of the methodology and the results of the aerodynamic analysis can be found in [1]. Only the summary results, i.e. the pressure coefficients and heat fluxes acting on the fairing along the trajectory, are given here and can be seen in Fig 3. From this figure it can be observed that the highest heat fluxes are expected to occur between Mach 2 and 7, i.e. between 29 and 56 seconds into flight. In order to evaluate the altitude influence onto the forces and momentum, simulations at high altitude were performed to evaluate the entire VBS-43 trajectory considering only zero angle of attack. In total eighteen points along the trajectory were selected considering both the effect of Mach number or altitude to correctly represent the various loads on the faring during the entire flight-path.

The force and moment coefficients for the different trajectory points are given in Table 2 and plotted in Fig 4. To compute the force and momentum coefficients acting in the fairing, the following was considered:

- Origin at [1.650, 0, 0] m;
- Reference area (base cone area): 1.4 m^2;
- Reference length (rolling momentum; base diameter D): 1.3356 m;
- Reference length (pitching momentum; model length L): 3.6500 m.

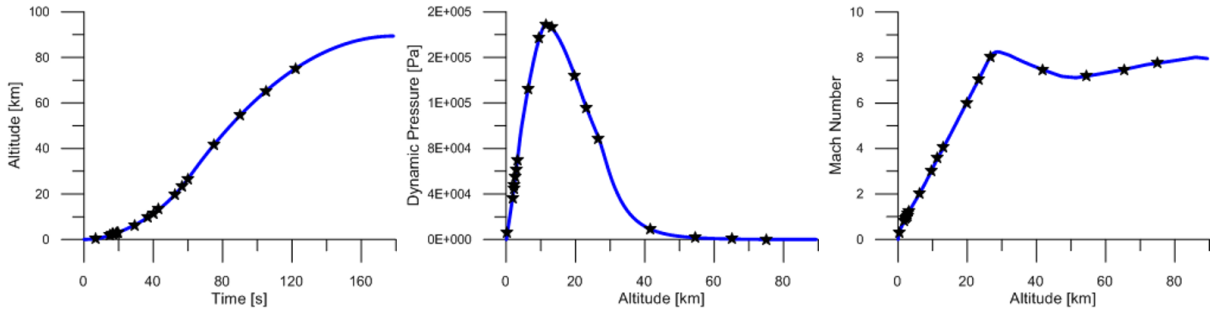

Fig 2. Trajectory analysis.

Table 1. *Critical aero-thermal load points along the flight path for numerical analysis*

Time [s]	Altitude [km]	Mach Number	Dynamic Pressure [Pa]	Reynolds number [1/m]
6.5	0.36	0.29	5.99E+03	6.60E+06
15.0	1.85	0.80	3.65E+04	1.56E+07
16.5	2.23	0.91	4.50E+04	1.71E+07
17.0	2.37	0.95	4.81E+04	1.76E+07
18.0	2.64	1.03	5.45E+04	1.86E+07
19.0	2.93	1.11	6.16E+04	1.96E+07
20.0	3.23	1.21	6.92E+04	2.35E+07
29.0	6.29	2.03	1.32E+05	2.57E+07
36.5	9.60	2.99	1.77E+05	2.64E+07
40.0	11.42	3.56	1.89E+05	2.51E+07
43.0	13.15	4.04	1.86E+05	2.17E+07
52.5	19.80	6.00	1.44E+05	1.14E+07
56.5	23.26	7.02	1.15E+05	7.60E+06
60.0	26.69	8.02	8.89E+04	5.04E+06
75.0	41.65	7.47	9.02E+03	4.59E+05
90.0	54.48	7.19	1.64E+03	8.39E+04
105.0	65.28	7.47	4.10E+02	2.36E+04
122.0	75.11	7.76	9.90E+01	6.36E+03

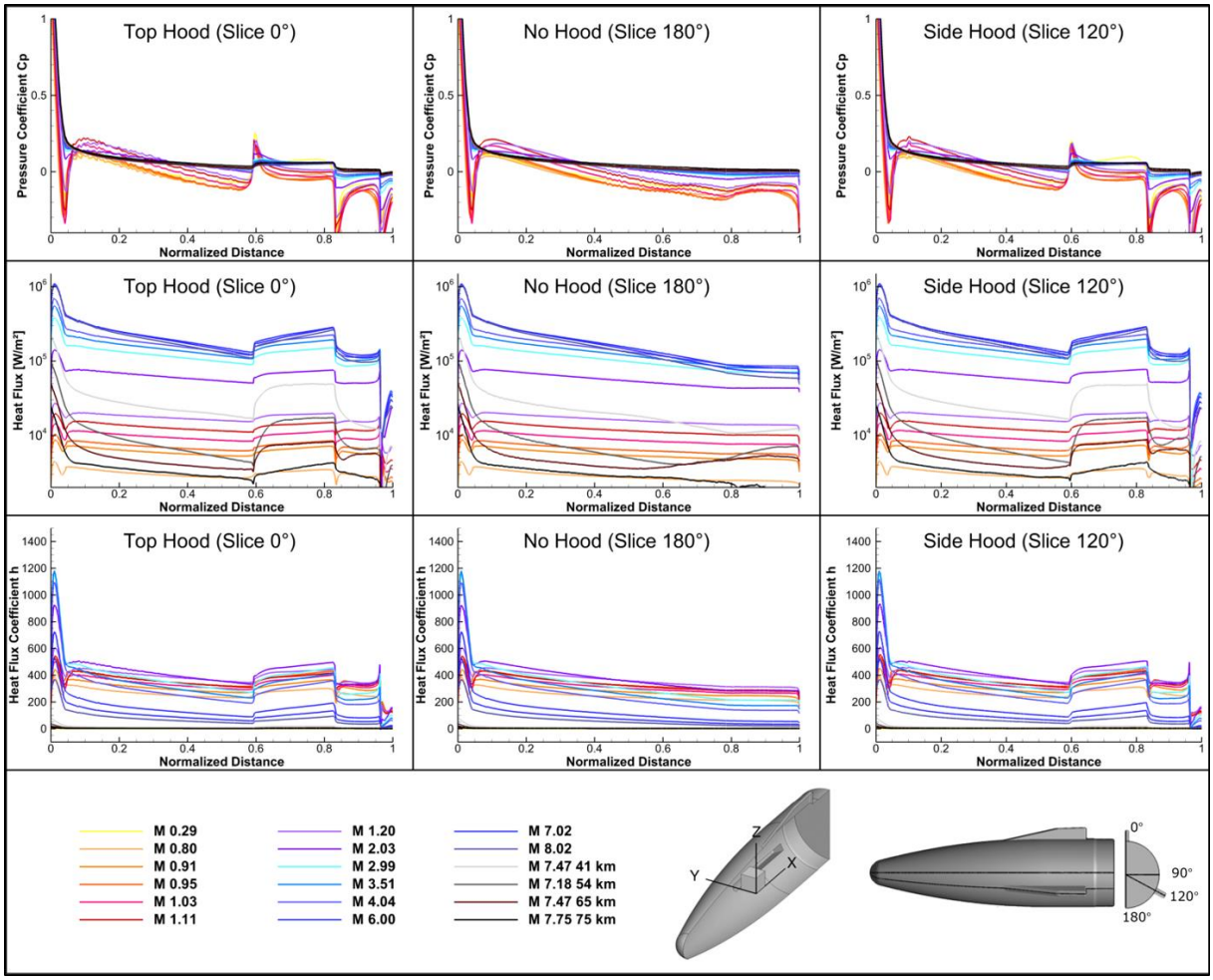

Fig 3. Pressure Coefficient, Heat Flux and Heat Flux Coefficient comparison along the trajectory.

Table 2. Forces and Momentum according to flight altitude.

Altitude	Angle of Attack	C-Lift	C-Drag	CM-x	CM-y	CM-z
0.36	0.00°	1.024E-05	1.161E-01	-1.342E-02	1.694E-04	0.00
1.85	0.00°	1.556E-04	7.510E-02	-1.732E-02	-2.545E-04	0.00
2.23	0.00°	5.250E-04	8.297E-02	-1.807E-02	-6.936E-04	0.00
2.37	0.00°	5.956E-04	9.080E-02	-1.822E-02	-7.723E-04	0.00
2.64	0.00°	4.263E-04	1.136E-01	-1.641E-02	-6.174E-04	0.00
2.93	0.00°	3.781E-04	1.344E-01	-1.323E-02	-5.453E-04	0.00
3.23	0.00°	-8.404E-05	1.460E-01	-1.185E-02	-1.456E-04	0.00
6.29	0.00°	-2.301E-04	1.427E-01	-5.131E-03	2.368E-05	0.00
9.60	0.00°	-6.157E-05	1.352E-01	-2.553E-03	2.797E-06	0.00
11.42	0.00°	-1.342E-04	1.320E-01	-1.710E-03	8.040E-05	0.00
13.15	0.00°	-8.343E-05	1.303E-01	-1.166E-03	3.597E-05	0.00
19.80	0.00°	-1.045E-04	1.261E-01	-8.211E-06	5.953E-05	0.00
23.26	0.00°	-1.019E-04	1.257E-01	2.869E-04	4.585E-05	0.00
26.69	0.00°	-9.984E-05	1.247E-01	4.794E-04	5.312E-05	0.00
41.65	0.00°	-1.757E-04	1.292E-01	4.003E-04	-1.339E-04	0.00
54.48	0.00°	2.381E-04	1.459E-01	5.707E-04	-1.132E-04	0.00
65.28	0.00°	6.087E-04	1.951E-01	1.214E-03	-5.062E-05	0.00
75.11	0.00°	3.489E-04	3.012E-01	1.986E-03	-3.505E-05	0.00

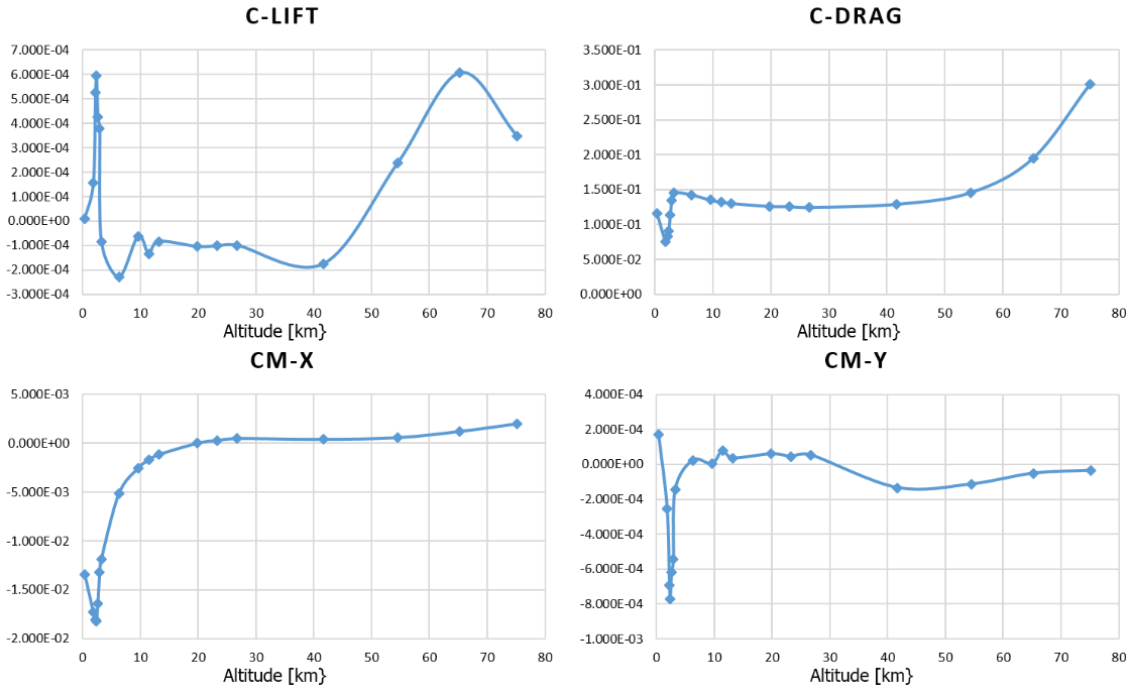

Fig 4. Forces and momentum in function of flight altitude.

3. Thermal Loads and Material Thickness Optimisation

The CFD simulations provide aerodynamic forces/moments and instantaneous heat flux values. However, in order to get the integrated heat loads, these heat fluxes need to be integrated over the complete trajectory and the heat balance of the material elements needs to be computed. For this purpose, the tool Pythelos (**Py**thon **The**rmal **L**oads **O**ptimisation **S**uite) was developed and applied to the fairing. The tool, for which a schematic of the workflow logic is shown in Fig 5, takes CFD data points of heat flux along the trajectory and integrates it to yield the heat loads. The tool can either compute the surface temperature at a specific instance during the ascent trajectory, or can be used to optimize the wall thickness to ensure it stays below a critical maximum temperature for assigned materials. In addition, Pythelos can automatically create input files and load cases for external structural solvers such as Nastran.

Pythelos takes into account convective heating and radiative cooling, but does not incorporate thermal conduction. Essentially each material element, defined by the elements of a surface triangulation, is solved as an independent zero-dimensional thermal node. It should thus be noted that this tool only gives a low-order estimation during design iterations, and does not replace the need for a full high-fidelity thermal analysis.

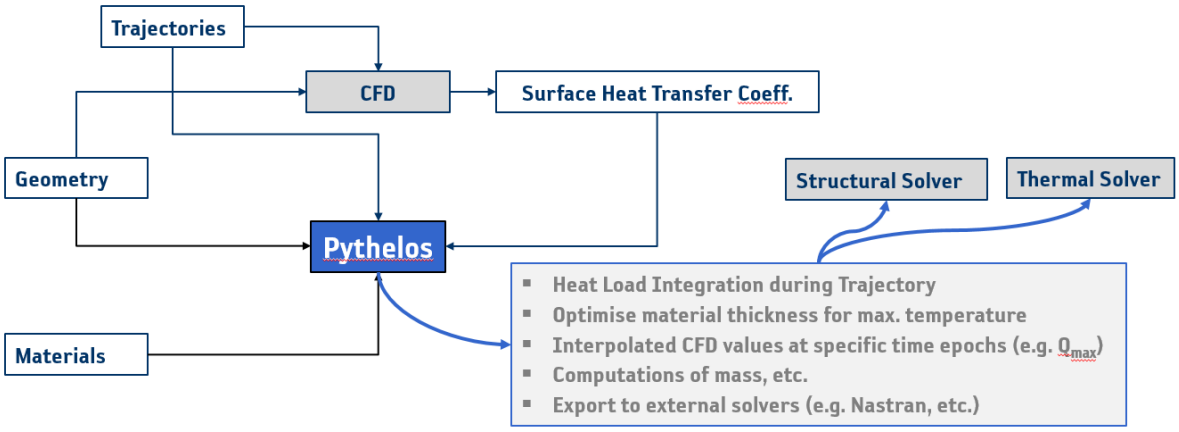

Fig 5. Schematic of the Pythelos workflow logic.

The tool has been applied to the hooded fairing discussed in the current work, and used the CFD data points presented in the previous section. Different materials were tested for different parts of the fairing (i.e. nosecone, fairing cylinder, and hoods) and the required minimum thickness to sustain the thermal loads was computed. Note that this minimum thickness serves as a starting point for further structural and thermal analyses, and does not necessarily mean the minimum thickness to survive structural loads. The material properties of the investigated materials are given in Table 3.

Table 3. Properties of the materials investigated with Pythelos.

Material	Density [kg/m³]	Spec. heat capacity [J/kg-K]	Emissivity [-]	Max. Temp. [K]
Titanium	4450	548-920	0.90	1070/870
Aluminium	2800	797-964	0.90	520
PEEK	1510	2160	0.75	420
Composite	1700	1100	0.75	520
Steel	7800	481	0.90	870
Inconel	8221	435	0.71	920

Notes: The maximum temperature for titanium at the nosecone was taken higher than at the rest of the fairing because the nosecone is mainly subjected to compressive loads and is therefore assumed to be less critical. For some metals the emissivity was assumed to be 0.90, as they will be coated with a black paint to enhance radiative properties.

The resulting minimum thickness of the walls to survive the integrated heat loads during the ascent are shown in Fig 6. From this figure it can be seen that small wall thicknesses can be achieved with titanium and steel, but that aluminium and the composite material need much thicker walls to handle the heat loading. As a result, the overall mass would be significantly higher for composite than for a titanium or steel, even though the material density is much lower. The masses of the nosecone, fairing cylinder and hoods for the different materials are given in Table 4. Note that these are masses computed with the minimum thickness required for the thermal load, not necessarily the overall resulting mass after a detailed structural and thermal analysis.

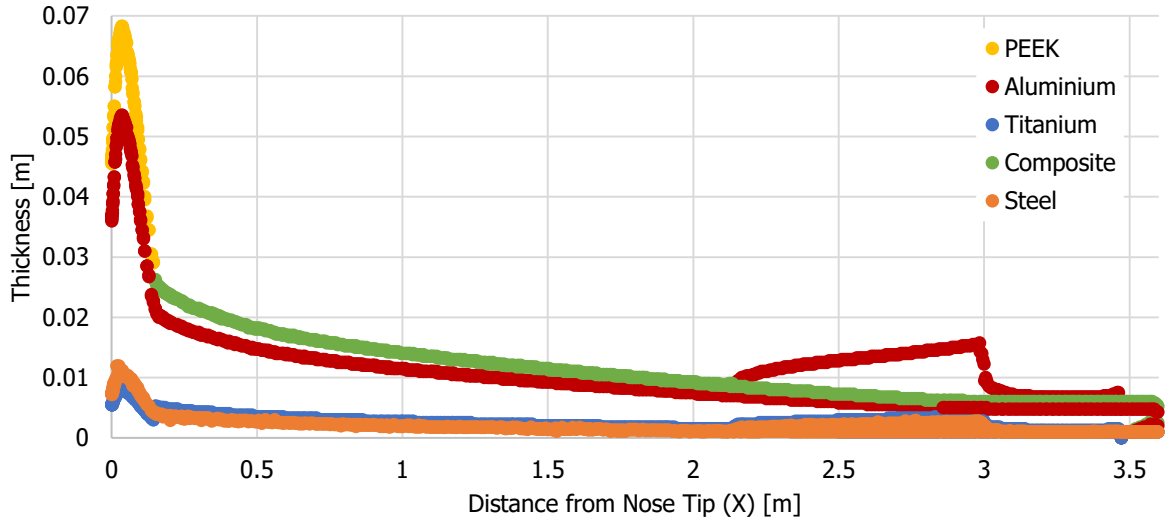

Fig 6. Minimum wall thickness along the fairing for different materials.

Table 4. Minimum mass of the fairing parts for different materials.

Mass [kg]	PEEK	Titanium	Aluminium	Composite	Steel	Inconel
Nosecone	14.8	5.0	21.4	-	12.0	-
Fairing	-	76.0	216.9	162.6	113.8	-
Hoods	-	10.8	31.3	-	14.9	15.6

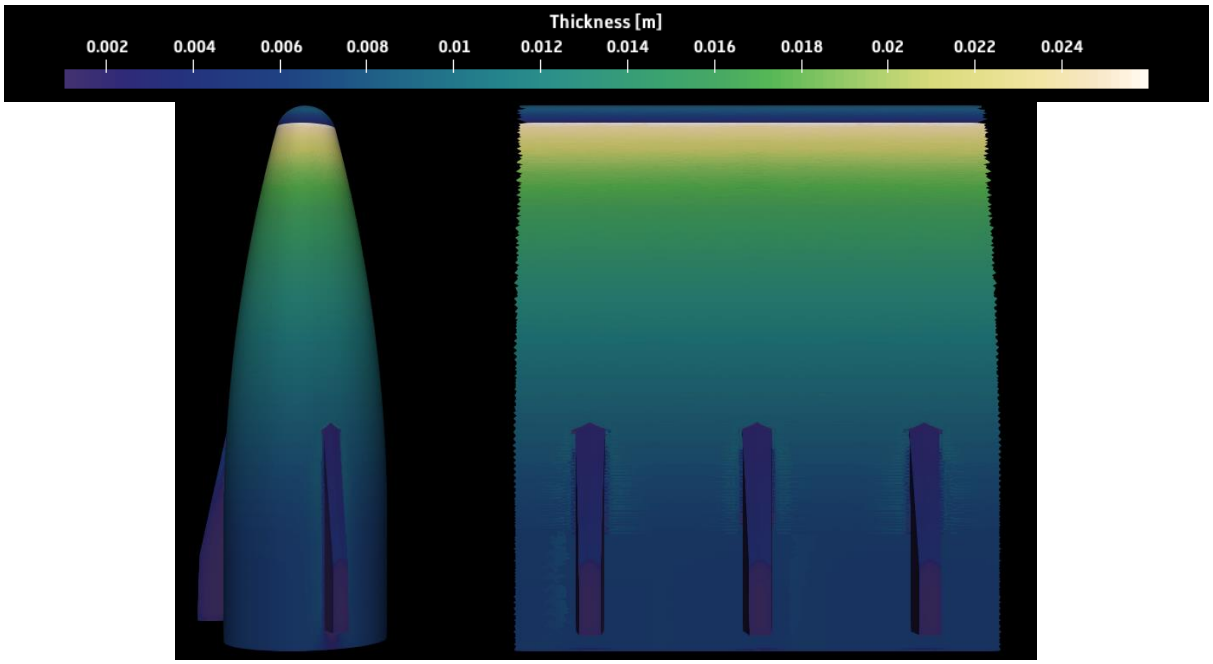

Fig 7. Material thickness for a titanium-composite-titanium fairing baseline.

As a baseline design, it was chosen to have a titanium nosecone, composite fairing cylinder and titanium hoods. The minimum thickness distribution of the fairing walls is shown in Fig 7. This baseline design was also used for the structural load analysis in the following section. The resulting temperature of this baseline fairing that is reached at the point of maximum dynamic pressure along the trajectory (Q_{max}) is shown in Fig 8.

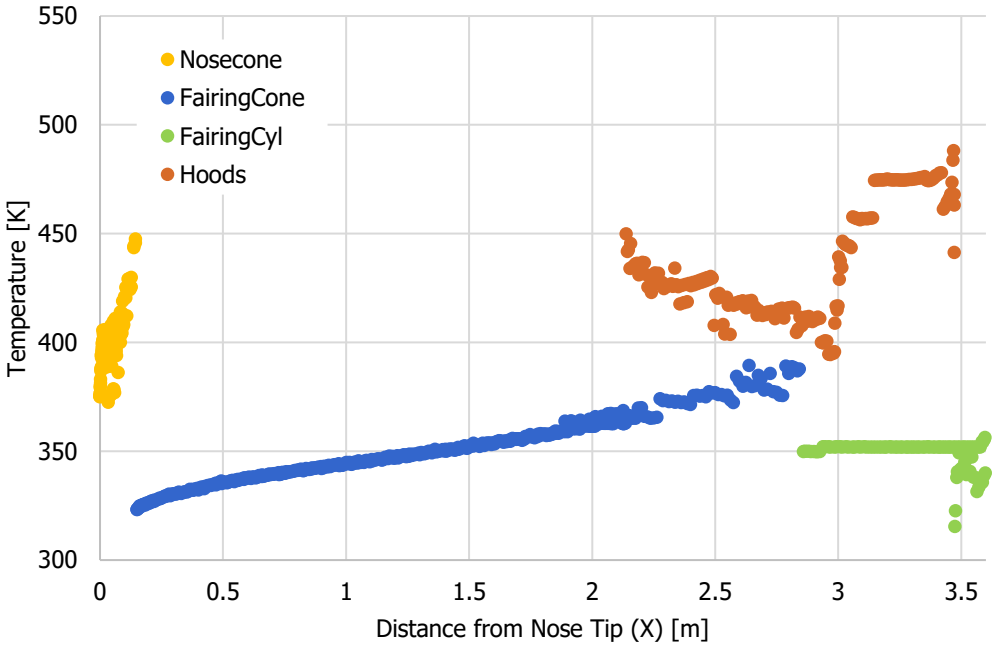

Fig 8. Temperature distribution along the titanium-composite-titanium fairing at Q_{max}.

4. Finite-element Analyses

Static loads and vibrational modes are computed by means of finite element analyses (FEA). The preliminary finite element model (FEM) of the fairing, which is used to aid the final design, is shown in Fig 9. The model is mainly composed of shell and solid elements. Additionally Multi-Point Constraints (MPC) are used at some interfaces. The thickness distribution and material properties (Fig 10) of the shell elements are exported from Pythelos directly into a Nastran file. It has been identified that the fairing shall be stiffened around the hoods in order to limit the deformations and stresses. The stiffening stingers of the FEM are depicted in Fig 11.

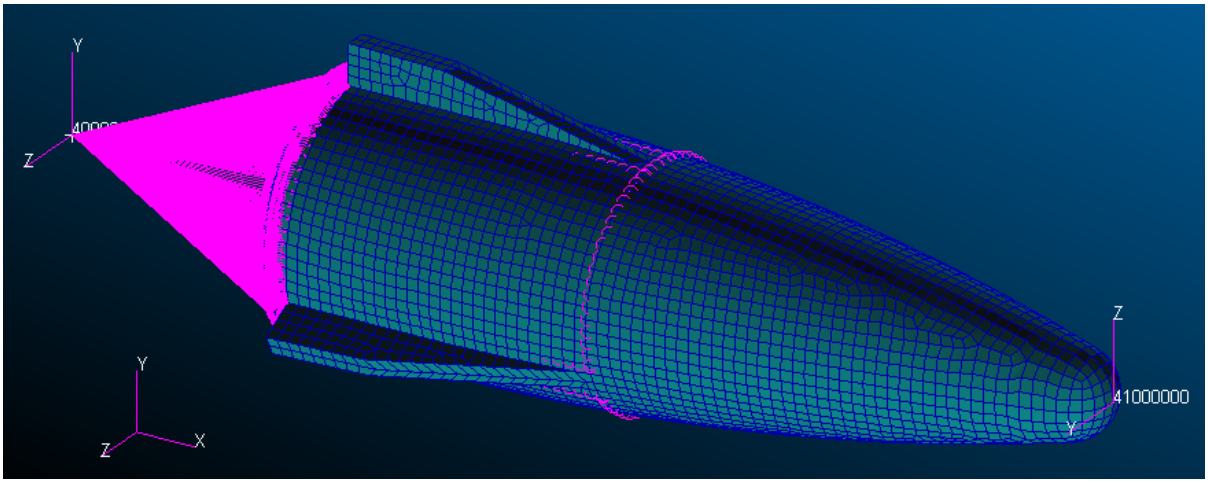

Fig 9. Finite Element Model of the fairing.

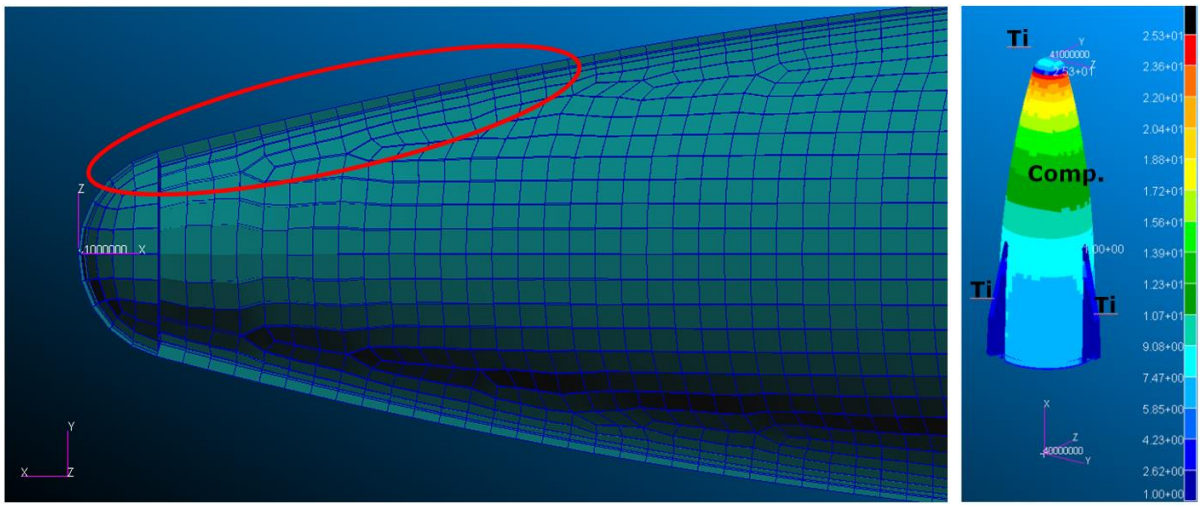

Fig 10. Variable thickness based on thermal calculations (left); materials (right)

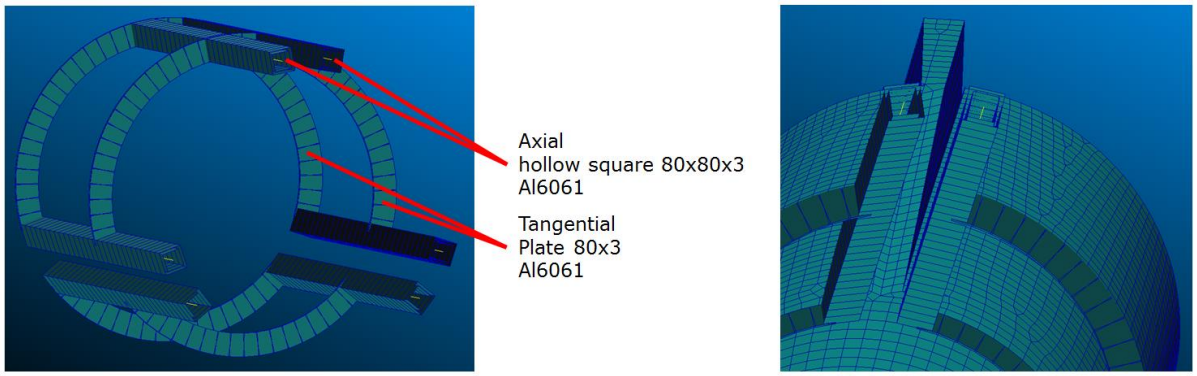

Fig 11. Stiffeners as built in the FEM.

Firstly, the fairing and then the EFTV-ESM-LVSM-Fairing stack has been analysed for normal modes. In the case of the fairing alone its interface towards the LVSM has been fixed in 6 DoF using a rigid RBE2 Nastran element. The first four modes are listed in Table 5. The first two lateral modes are depicted on Fig 12. Secondly, the fairing has been attached to the LVSM-ESM-EFTV stack and a normal modes analysis was run. The bottom interface of the LVSM has been fixed. The first four modes are listed in Table 6, and the corresponding mode shapes are depicted in Fig 13.

Table 5. Eigenmodes of the fairing.

Mode	Frequency (Hz)	Description
1	38.2	Up-down
2	38.8	Sideways
3	71.7	Wing hoods twisting
4	72.1	Sides in and out

Table 6. Eigenmodes of the EFTV-ESM-LVSM-Fairing stack.

Mode	Frequency (Hz)	Description
1	8.9	EFTV sideways
2	9.3	EFTV up-down
3	23.8	Fairing+EFTV sideways
4	24.0	Fairing+EFTV sideways up-down

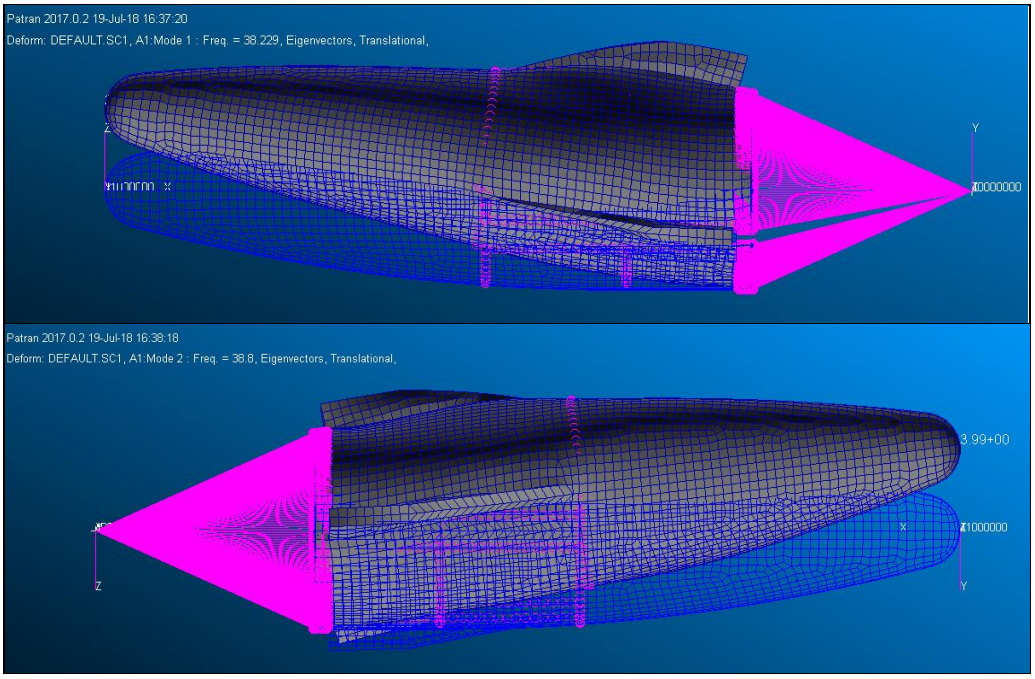

Fig 12. First two eigenmodes of the fairing.

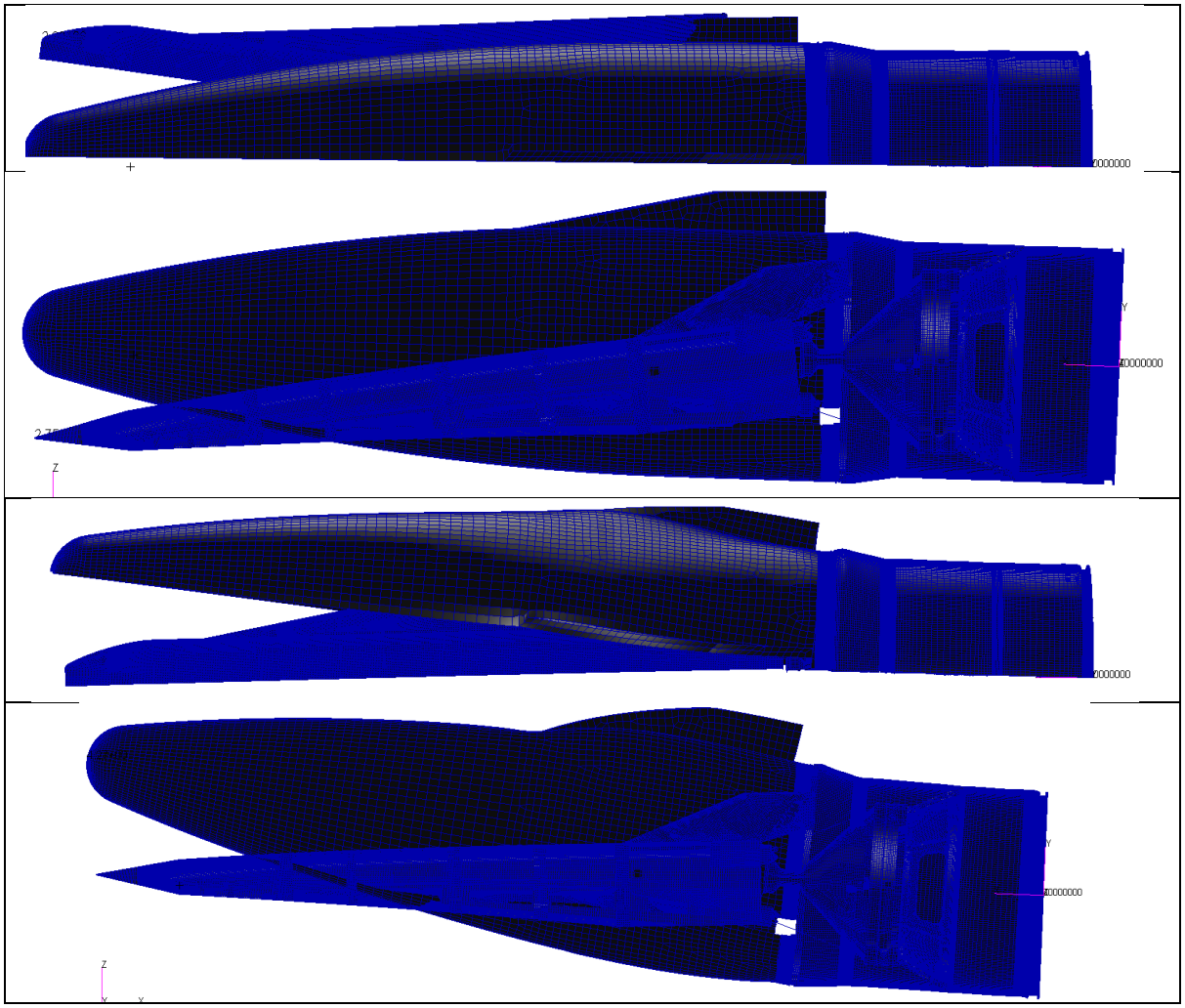

Fig 13. Mode shapes of the EFTV-ESM-LVSM-Fairing stack. Top-to-bottom: Mode 1, 2, 3, 4.

Static loads analyses were performed in order to aid the final design of the fairing. Quasi-static, pressure and temperature loads have been applied on the model at the same time for two load cases: Transonic and maximum dynamic pressure (Q_{max}). The quasi-static loads are represented as acceleration, while pressure and temperature loads are mapped to the Nastran mesh using Pythelos. The deformed shape of the fairing is shown in Fig 14 for the two load cases.

The von Mises stress distribution has also been calculated for the two load cases, shown in Fig 15. Stress concentration is visible at the front part of the fairing where there is a discontinuity in the composite thickness and around the hoods, which are from a different material than the rest of the fairing.

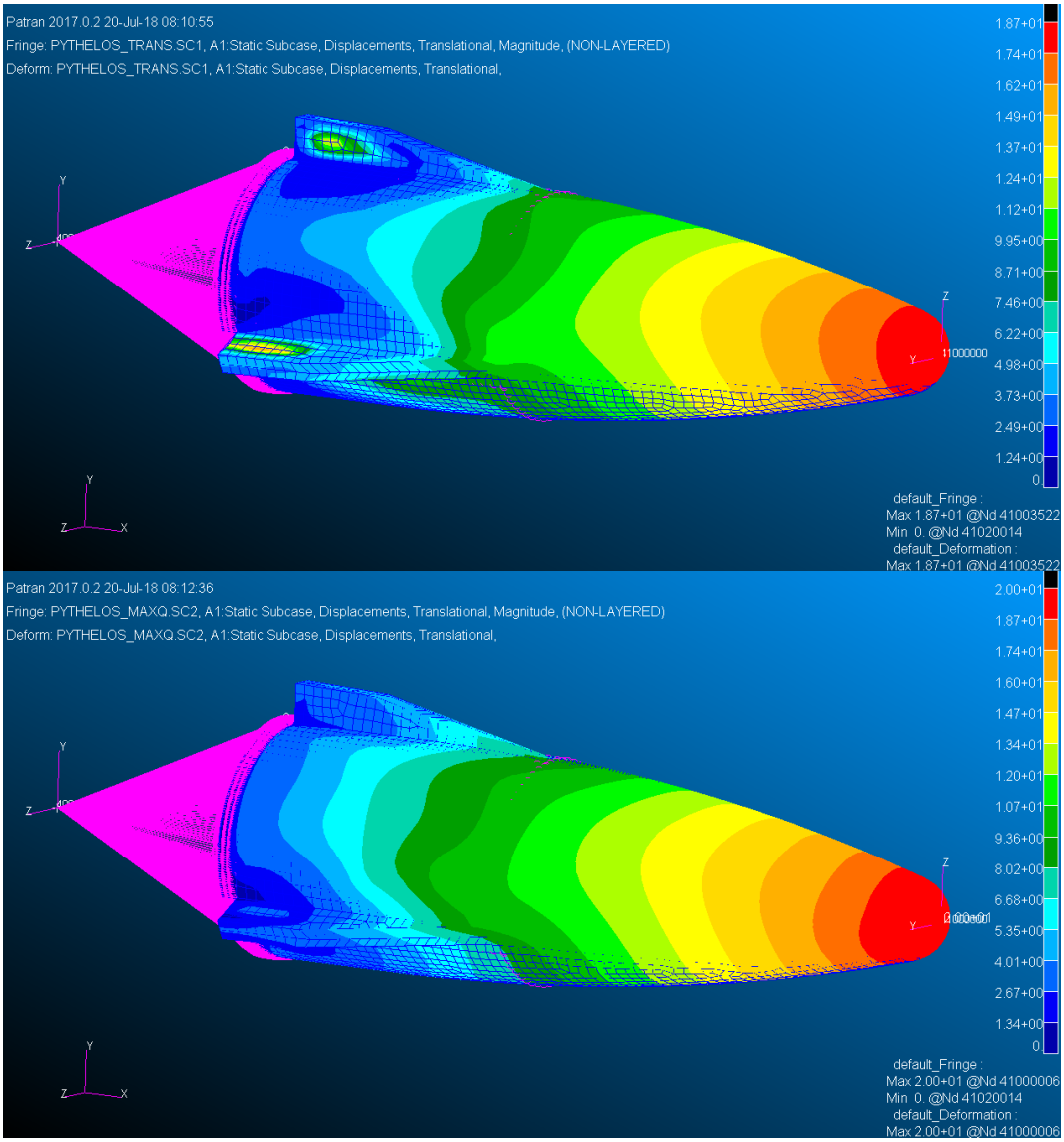

Fig 14. Magnitude of deformation (in millimetres). Top: transonic load case; bottom: Q_{max} load case

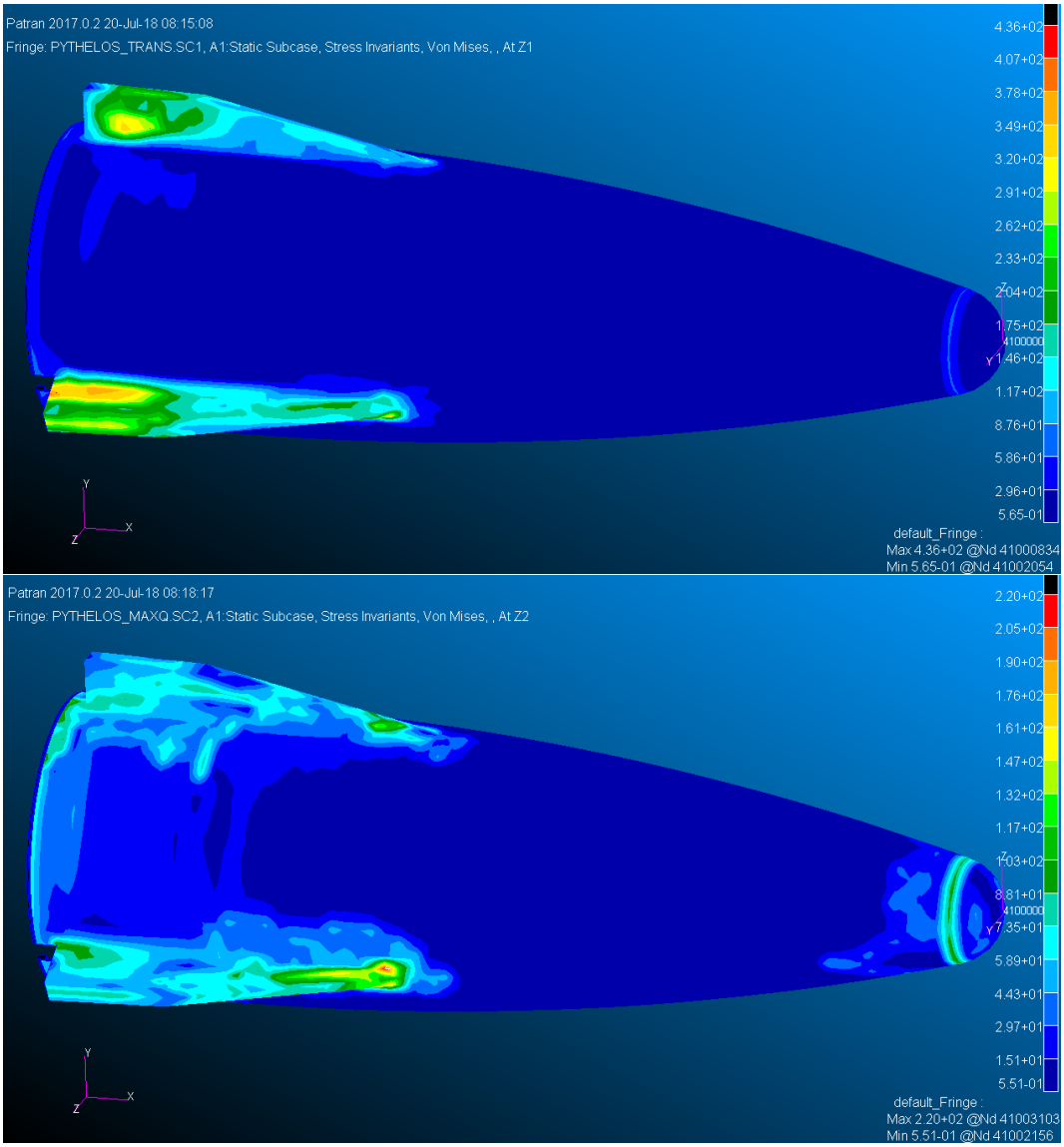

Fig 15. Von Mises stress in the two load cases. Top: transonic load case; bottom: Q_{max} load case

5. Manufacturing

The starting point of the material selection for the fairing is the use of a glass-fibre composite, produced by vacuum infusion method. This allows to optimize the fairing structure with variable skin thickness and stiffeners following mass limit and stiffness distribution (Fig 16). Other materials will be considered at local hot spots depassing the glass fibre composite operational temperature. This is expected to happen at the nose-tip and along the leading edges of the hoods. For the nose tip, PEEK as a solid block is considered allowing easy mounting (Fig 17). For the hoods, CFRP or metallic casings are considered which are easily mountable on the composite fairing.

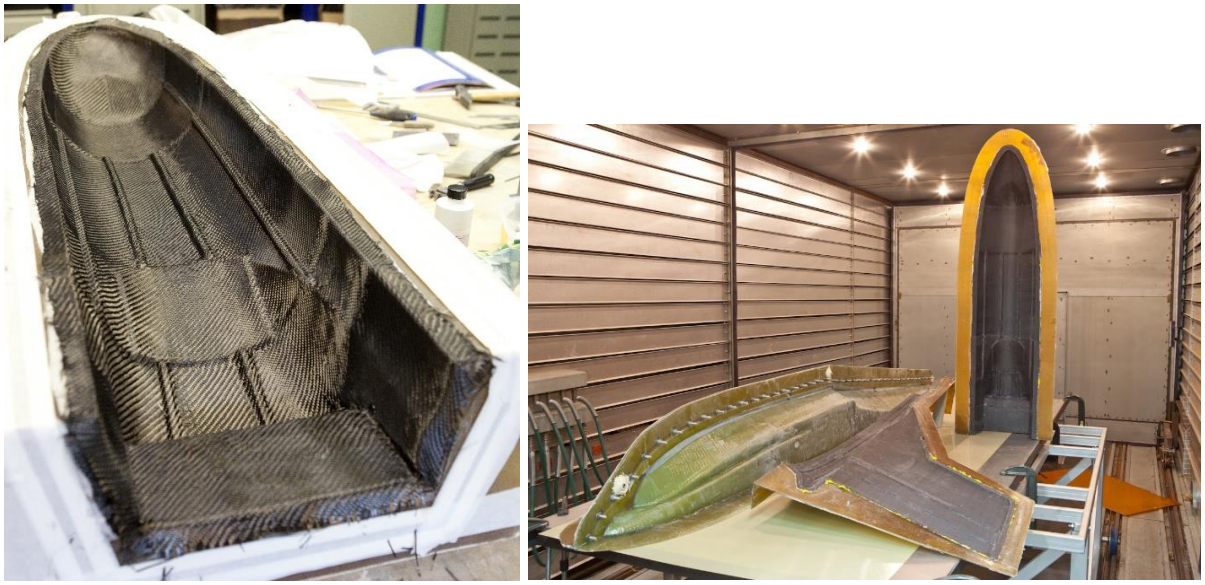

Fig 16. Customize fibre glass cone with variable thickness skins and embedded stiffeners (left) and customized protrusions (right).

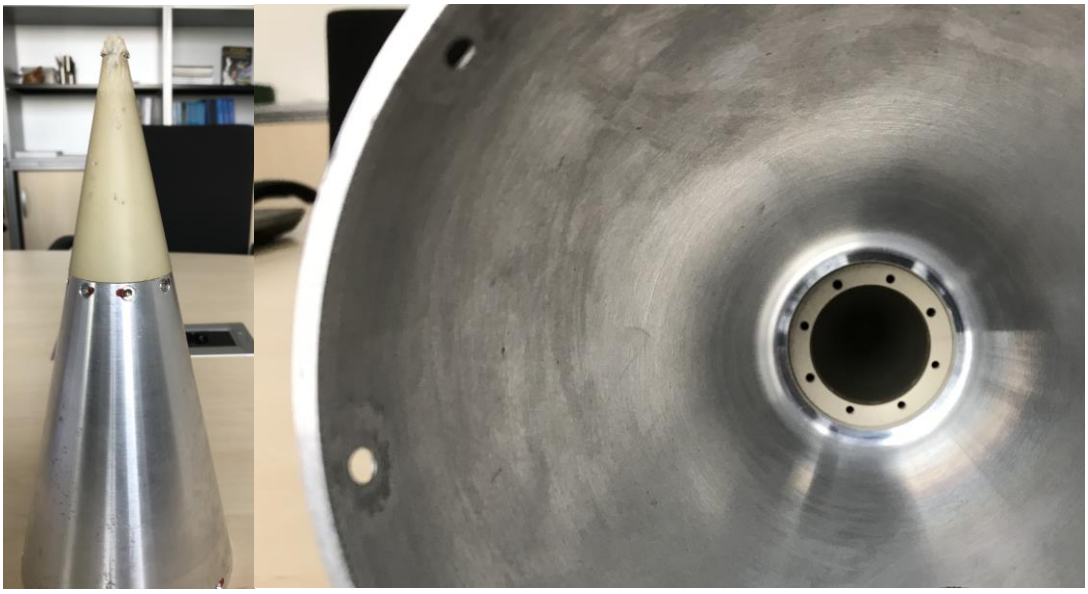

Fig 17. PEEK nose tip mounted on aluminum cone:
external view (left), internal mounting with aluminum shoulder (right).

Fig 18 gives the general layout of the composite fairing. The overall body skin consists of 6 composite petals and six ring-shaped frames. The division into 6 composite petals makes the tooling impact lower and simplifies the manufacturing process. Three petals are closed, whereas the three intermediately placed petals have open slits at the location of the hoods. The composite petals are connected/glued to each other by inner folded ribs offering longitudinal stiffness. The first frame offers the possibility to mount the nose tip, whereas the lowest frame has a profiled ring to be mated with the launch vehicle by a clamp band. The metallic hoods are integrated into 3 petals.

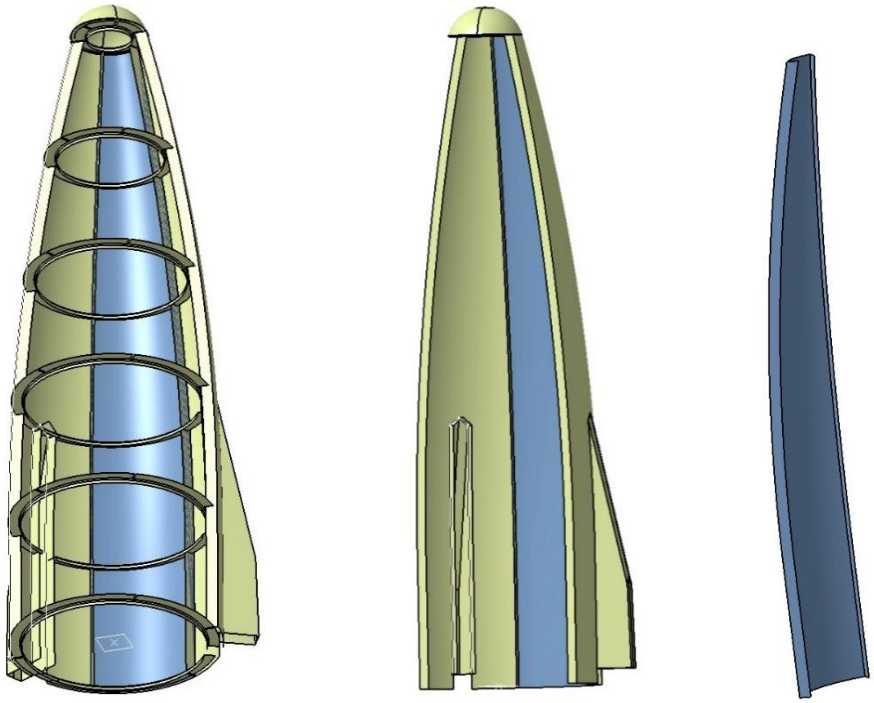

Fig 18. General layout and composition of composite fairing.

6. Conclusions

The present paper described a preliminary design methodology which was applied for a complete analysis loop for a hooded fairing. Based on the mission scenario of HXI for the VBS-43 ascent trajectory, different flight segments were numerically analysed with CFD. Aerodynamic loads and heat fluxes were computed at discrete point along the trajectory. A tool was developed to compute the overall integrated thermal load during the ascent, and optimise the wall thickness of the fairing to sustain this load. The considered materials were either metallic or composite whereas the use of sandwich panels or CFRP was not yet considered. Apart from high-emissivity paint, no consideration of other thermal protection system, such as phenolic cork [8] were considered. This preliminary wall thickness distribution was then used as input to a structural FEM analysis. Finally, some notes on the manufacturing were presented.

Acknowledgements

This work was performed within the 'High Speed Experimental Fly Vehicles - International' project fostering International Cooperation on Civil High-Speed Air Transport Research. HEXAFLY-INT, coordinated by ESA-ESTEC, is supported by the EU within the 7th Framework Programme Theme 7 Transport, Contract no.: ACP3-GA-2014-620327 and by the Ministry of Industry and Trade, Russian Federation. Further info on HEXAFLY-INT to be found on http://www.esa.int/techresources/hexafly_int.

João F. A. Martos would like to thank ESA for receipt of the International Research Fellowship in the framework of international collaboration between ESA and Brazil.

References

1. João F. A. Martos , Rafael O. Santos, Marco A. S. Minucci, Israel S. Rego and Steelant J., 'Aerodynamic Characterization of a Hooded Fairing Accommodating Winged Payloads', 1st International Conference on High-Speed Vehicle Science and Technology (HiSST), 26-29/11/2018, Moscow, Russia.

2. A. Paull, H. Alesi and S. Anderson, 'The Development of the HyShot Flight Program', in: Jiang Z. (eds) Shock Waves. Springer, Berlin, Heidelberg, pp. 31-48, 2005.

3. Eggers Th., Longo J., Turner J., Jung W., Hörschgen M., Stamminger A., Gülhan A., Siebe F., Requardt G., Laux T., Reimer T. and Weihs H., 'The SHEFEX Flight Experiment - Pathfinder Experiment for a Sky Based Test Facility', 14th AIAA/AHI Space Planes and Hypersonic Systems and Technologies Conference, Canberra, Australia, AIAA 2006-7921.

4. Eggers Th., 'The SHEFEX II Experimental Re-Entry Vehicle: Presentation of Flight Test Results', 28th Int. Congress of the Aeronautical Sciences, 23 - 28 September, 2012, Brisbane, Australia

5. Dolvin D.J., 'Hypersonic International Flight Research and Experimentation (HIFiRE): Fundamental Sciences and Technology Development Strategy', 15th AIAA International Space Planes and Hypersonic Systems and Technologies Conference, 28 April - 1 May 2008, Dayton, Ohio, AIAA-2008-2581

6. Steelant, J., Langener, T., Hannemann, K., Riehmer, J., Kuhn, M., Dittert, C., Jung, W., Marini, M., Pezzella, G., Cicala, M., Serre, L.: Conceptual Design of the High-Speed Propelled Experimental Flight Test Vehicle HEXAFLY. In: 20th AIAA International Space Planes and Hypersonic Systems and Technologies Conference, 5-8 July, Glasgow, Scotland, AIAA-2015-3539, (2015)

7. Steelant J., Marini M., Pezzella G., Reimann B., Chernyshev S.L., Gubanov A.A., Talyzin V.A., Voevodenko N.V., Kukshinov N.V., Prokhorov A.N., Neely A.J, Kennel C., Verstraete D., Buttsworth D., 'Numerical and Experimental Research on Aerodynamics of High-Speed Passenger Vehicle within the HEXAFLY-INT Project', 30th Congress of the International Council of Aeronautical Sciences (ICAS), 25-30/09/2016, Daejeon, Korea.

8. Drescher, O., Hörschgen-Eggers, M., Pinaud, G. and Podeur M., `Cork Based Thermal Protection System for Sounding Rocket Applications – Development and Flight Testing, 23rd ESA PAC Symposium, 11.-15. Jun. 2017, Visby, Schweden

